Journal of Advanced Research 25 (2020) 181–189

Contents lists available at ScienceDirect

Journal of Advanced Research

journal homepage: www.elsevier.com/locate/jare

Research Article

Iso-damping fractional-order control for robust automated car-following

Carlos Flores [a,*], Jorge Muñoz [b], Concepción A. Monje [b], Vicente Milanés [c], Xiao-Yun Lu [a,d]

[a] California PATH Program of the Institute of Transportation Studies, University of California Berkeley, Richmond, CA 94804, United States
[b] University Carlos III of Madrid, Systems Engineering and Automation Department, Avenida Universidad 30, 28911 Leganés, Madrid, Spain
[c] Research Department, Renault SAS, 78280 Guyancourt, France
[d] Lawrence Berkeley National Lab, Berkeley, CA 94720, United States

HIGHLIGHTS

- Novel control design method for fractional-order controllers for more demanding design requirements.
- A more graphical approach to tune fractional-order controllers, easing the control system deployment on any type of vehicles.
- Application of such design approach to real world problems and real vehicles platforms.
- A method to guarantee iso-damping properties, which is essential for automated car-following.

GRAPHICAL ABSTRACT

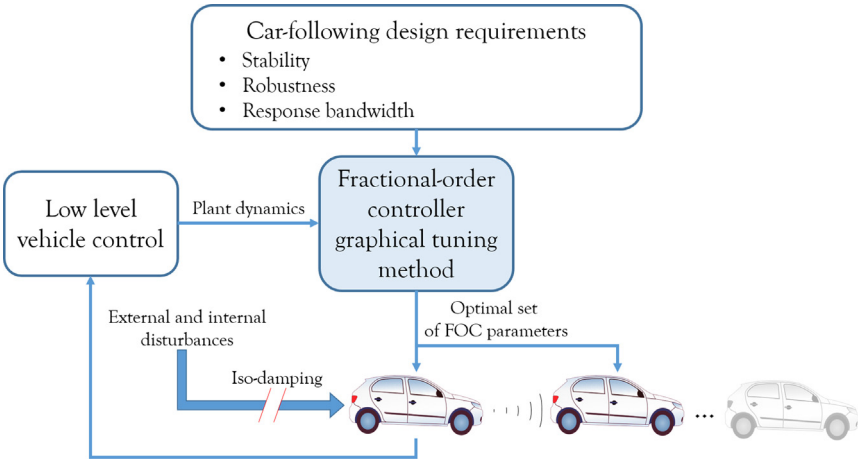

ARTICLE INFO

Article history:
Received 20 March 2020
Revised 7 May 2020
Accepted 13 May 2020
Available online 17 June 2020

Keywords:
Fractional-order control
Adaptive cruise control
Iso-damping stability
Intelligent transportation systems

ABSTRACT

This work deals with the control design and development of an automated car-following strategy that further increases robustness to vehicle dynamics uncertainties. The control algorithm is applied on a hierarchical architecture where high and low level control layers are designed for gap-control and desired acceleration tracking, respectively. A fractional-order controller is proposed due to its flexible frequency shape, fulfilling more demanding design requirements. The iso-damping loop property is sought, which yields a desired closed-loop stability that results invariant despite changes on the controlled plant gain. In addition, the graphical nature of the proposed design approach demonstrates its portability and applicability to any type of vehicle dynamics without complex reconfiguration. The algorithm benefits are validated in frequency and time domains, as well as through experiments on a real vehicle platform performing adaptive cruise control.

Introduction

Traffic congestion remains as one of the biggest problems in cities, with Los Angeles representing the worst-case scenario where commuters lose up to 119 h per year [1]. Traffic jams are not only impacting wasted time but also pollution with 12.5 billion extra gas liters

Peer review under responsibility of Cairo University.

* Corresponding author.
E-mail addresses: carfloresp@berkeley.edu (C. Flores), jmyanezb@ing.uc3m.es (J. Muñoz), cmonje@ing.uc3m.es (C.A. Monje), vicente.milanes@renault.com (V. Milanés), xiao-yun.lu@berkeley.edu (X.-Y. Lu).

https://doi.org/10.1016/j.jare.2020.05.013
2090-1232/

consumed due to traffic only in America in 2017 [1]. These figures clearly point out to a real world problem where control systems applied to vehicles may significantly improve current numbers.

The application of intelligent control algorithms to ground transportation systems are widely known as Advanced Driving Assistance Systems (ADAS). Among the different systems, the ability to automatically control both throttle and brake pedals simultaneously is known as Adaptive Cruise Control (ACC) [2]. ACC is set to track a desired speed, unless a target vehicle is detected and the setpoint speed is changed to maintain a safe gap accordingly. Former studies have already demonstrated the benefits of ACC in reducing pollution [3]. However, commercially available ACC systems have been mainly oriented as a comfort feature for high-end vehicles, with little implications in the traffic flow, yielding zero traffic improvement even considering 100% market penetration [4]. Recent studies have demonstrated that production systems (mainly based on PD controllers) exhibit some performance limitations when coping with all ACC control requirements, showing the need of more advanced control structures to deal with more demanding specifications [5].

Almost all of the control systems deployed in industrial applications utilize controllers with the PID frequency shape [6]. When it comes to developing production ACC systems, classical PD control structures remain the most commonly applied control technique. The main reason is its easy-to-tune capabilities when transferring the control design to a real world implementation. However, more complex control structures have been applied for ACC. Among them, Model Predictive Control (MPC) for improving not only car-following capabilities but also HEV energy optimization is presented in [7]. A comparison regarding tracking error and control effort between a model-free control technique and a fuzzy logic approach is presented in [8] for Stop&Go maneuvers. Robust control is applied in [9] by using the H_∞ norm to consider vehicle dynamics uncertainties, leading to an off-line optimization control problem. The main limitation of these techniques is the complexity of the tuning process, which is a main issue when considering implementation on real platforms.

Fractional-order control provides a good balance between dealing with a more demanding control structure and keeping simplicity and easy-to-tune capabilities. Fractional-order calculus has been already applied in the automotive domain for the design of vehicle suspension systems [10]. From the intelligent transportation perspective, it has been applied to both lateral and longitudinal autonomous vehicle control problems. A fractional-order PID algorithm for precise lateral control in parking maneuvers is presented in [11]. Full-speed lateral fractional controller is explored in [12] where the relationship between vehicle speed and the fractional-order of the controller is studied. A cruise control system for low-speed gas-propelled vehicle based on a fractional-order PI controller is presented in [13]. Hosseinnia et al. [14] showed a hybrid fractional ACC controller for low speeds but the design takes into account neither the traffic flow improvement nor a methodology to guarantee easy-to-tune capabilities.

Classic fractional-order controllers tuning algorithms can be based on analytical methods, as in [15–18]; or optimization, as in [19,20]. Some works have also proposed auto-tuning algorithms to dynamically set the fractional-order controller parameters [21–25]. The main limitation of the majority of these algorithms lies in the dependency of numeric and optimization solvers which are highly dependent on initial conditions and may converge in local minima. Having this in mind, an approach able to provide visual cues about how each optimal parameter contributes to the loop dynamics performance can significantly help on the controller design.

Graphical methods to solve equation systems (linear and nonlinear) have gained a lot of attention and are thoroughly used, even within the fractional-order control field [26–28]. However, these approaches not only rely on a highly complex graphical representation, but also require complete reset of the algorithm if control requirements or problem conditions are changed. Recently, a counter-slope method has been proposed to overcome this limitation [29]. Here, the proposed graphical method offers a better insight of the controller parameters effect on the system response.

In this paper, a fractional-order control design methodology is presented that enhances the method in [29], by allowing the selection of the loop phase margin and crossover frequency, while guaranteeing the loop iso-damping property. It uses a more intuitive graphical representation that shows all possible controller tuning possibilities. This not only permits to tune controller parameters in a more straightforward manner, but also avoids issues related to local minima. Consequently, the method can be more easily adapted to any type of system dynamics, which results ideal to encourage widespread commercial adoption of automated car-following technologies. As computational effort is drastically reduced compared to the aforementioned methods, this approach can be deployed in low power embedded hardware platforms, reducing weight, energy and cost and making it an optimal solution for real embedded ACC applications.

The rest of the paper is structured as follows. Section "Car-following framework" introduces the car-following framework upon which the control algorithm is applied, including the experimental platform characteristics and its longitudinal model. Section "Gap controller design" presents the fractional-order ACC control design with traffic flow and easy-to-tune considerations. Section "Simulation results" shows frequency and time domains validation of the control system in simulation and further on, in Section "Experimental results" experiments on a real vehicle demonstrate the algorithm effectiveness. Finally, some concluding remarks are given in Section "Conclusions and future works".

Car-following framework

The ACC framework used in this work is presented in Fig. 1. Its subsystems are hierarchically designed with different performance objectives. For the sake of clarity, variables and blocks belonging to the subject vehicle are indexed with subscript i, where $i \in [1, N]$, N being the size of the controlled string of vehicles. The structure depicted in Fig. 2 is based on a cascade approach where the low level structure deals with the reference acceleration tracking task, while the high level control is designed to regulate the distance gap with respect to the preceding vehicle.

The low level control $Gp_i(s)$ comprises the system that manages throttle and brake actuators to track a given reference acceleration generated by the high level layer. The vehicle's position and velocity are fed back and used to define the desired distance gap. This is done following the set spacing policy, which in this work is a constant time gap [30]. It consists on keeping a fixed safety distance added to a time gap h that multiplies the subject vehicle speed. This policy not only increases loop stability by adding a zero on the feedback loop represented as $H_i(s) = hs + 1$, but also fits the best the way human drivers perform car-following. The spacing error $E_i(s)$ between measured and desired gap is processed by the controller $C_i(s)$ to generate the high level control action $u_i(t)$. This signal is added as a correction to the vehicle longitudinal speed to define the reference acceleration to be tracked by low level control layer $Gp_i(s)$.

Low level control layer

The design objectives for the reference acceleration tracking block $Gp_i(s)$ are as follows: (1) accurate and consistent tracking

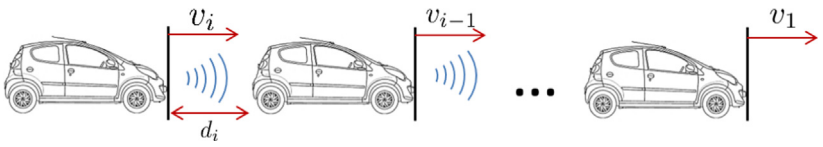

Fig. 1. Illustration of an ACC-controlled vehicle string.

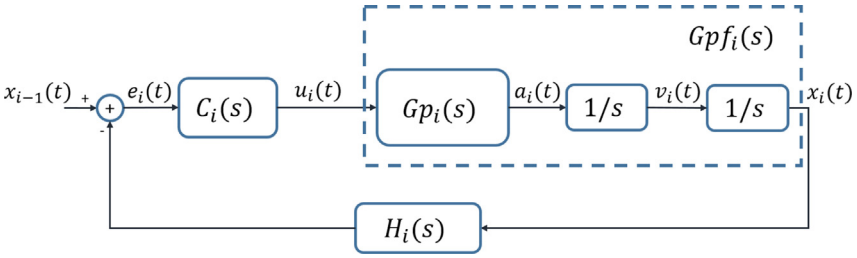

Fig. 2. Block representation of the hierarchical car-following structure.

of the given reference acceleration; and (2) adaptability and robustness to different types of vehicles and road conditions. By ensuring fulfillment of both conditions, a more suitable low level behavior model is available for further design of the high level structure, reducing model response uncertainties. The vehicle longitudinal motion $a_i(t)$ is modeled as:

$$M_v a_i(t) = \frac{\tau_{th,i}(t) - \tau_{br,i}(t)}{r_w} - F_a(\dot{x}_i(t)) - F_g(\theta_r) - F_r(\theta_r, \mu), \tag{1}$$

where $M_v, r_w, \theta_r, \mu, \tau_{th,i}(t)$ and $\tau_{br,i}(t)$ stand for the vehicle mass, wheel radius, road steepness and friction; motor propulsion and braking torques, respectively [31]. Disturbances on the vehicle body are given by the aerodynamic resistance F_a, the gravitational force F_g and the rolling resistance force F_r. The low level layer is designed to track the reference acceleration by acting on the throttle and brake system torques, $\tau_{th,i}(t)$ and $\tau_{br,i}(t)$, respectively.

Through extensive open-loop testing and modeling of throttle and brake actuators, the effect of their application levels on the longitudinal acceleration can be mapped in function of the vehicle velocity. This permits to select the ideal throttle or brake pedal deflection required to generate the desired longitudinal torque at the measured longitudinal speed. Fig. 3 illustrates the low level control structure $Gp_i(s)$, where systems $G_{th,i}(s)$ and $G_{br,i}(s)$ stand for the throttle and brake systems' transfer functions:

$$\begin{aligned} G_{th,i}(s) &= \frac{\tau_{th,i}}{u_{th,i}} = \frac{K_{th}}{s/\omega_{th}+1}; \\ G_{br,i}(s) &= \frac{\tau_{br,i}}{u_{br,i}} = \frac{K_{br}\omega_{br}^2}{s^2+2\xi_{br}\omega_{br}s+\omega_{br}^2}; \end{aligned} \tag{2}$$

The high level control action is processed by controller $C_{ll,i}(s)$ to generate a desired acceleration $a_{ref}(t)$. This control action is passed through the modelled throttle and brake maps, obtaining the desired throttle or brake levels, $u_{th,i}$ and $u_{br,i}$, respectively; for the current ego-speed.

The design of the controller $C_{ll,i}(s)$ must ensure low loop sensitivity in the frequency spectrum of vehicle external disturbances F_a, F_g and F_r (usually low to medium frequencies). The loop response shape is desired with high gain for low frequencies, stability with feasible response bandwidth at medium frequencies and low gain at high frequencies for noise rejection [32]. In this work, the actuators' maps and the low level control layer are designed for the dynamics of a Hybrid Honda Accord 2014. A reference acceleration profile is designed to analyze and model the low level control layer performance. Fig. 4 shows the response of the system $Gp_i(s)$. Stabilization time towards reference speed changes results consistent, whether it is applying throttle or brake, demonstrating the closed-loop stability and showing the effectiveness of having throttle and brake maps to select ideal actuation for the desired acceleration/deceleration.

However, a slight error is observed as vehicle speed does not fully converge to the reference in steady state, which is due to unmodeled dynamics that can be expressed as DC gain disturbances. Considering this behavior, data from this experiment is used to model the low level control dynamics $Gp_i(s) = A_i(s)/U_i(s)$, yielding:

$$Gp_i(s) = \frac{A_i(s)}{U_i(s)} = \frac{\Delta \cdot 4.51}{s + 3.717}, \tag{3}$$

where the parameter Δ represents the possible plant DC gain disturbance, which has a nominal value of 1. This parameter models possible changes on the vehicle mass or road slope, given that these disturbances occur in the low frequency spectrum. These disturbances are modeled in Fig. 3 as the block Δ. Robustness against these uncertainties is targeted in the design of the high level gap-regulation controller $C_i(s)$, together with gap-regulation stability and response bandwidth requirements.

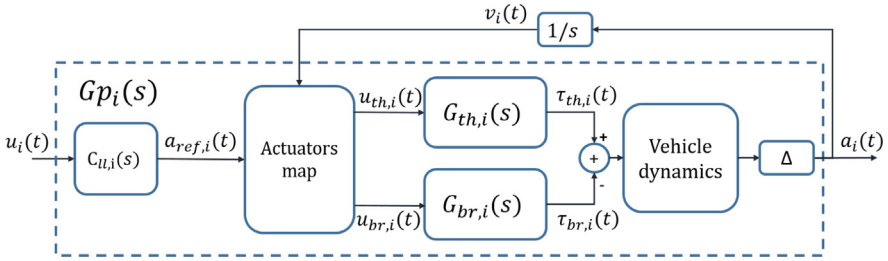

Fig. 3. Block diagram of the speed tracking control layer $Gv_i(s)$.

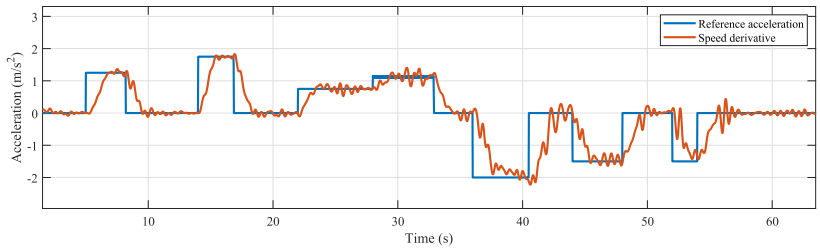

(a) Acceleration response to designed acceleration profile

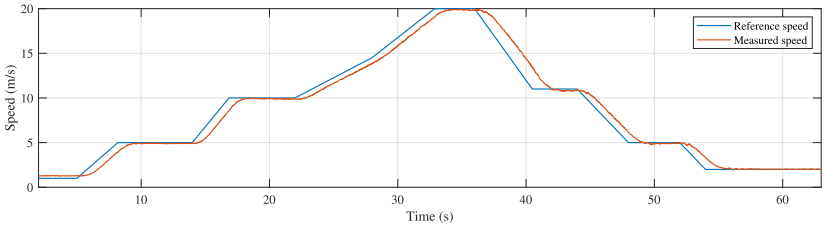

(b) Speed response to speed profile

Fig. 4. Performance study for the designed low level block $Gp_i(s)$.

Gap controller design

The control design is focused on stabilizing the external feedback loop in Fig. 2. Phase margin and stability metrics are measured on the open loop expression $L_i(s) = C_i(s)Gpf_i(s)H_i(s)$, where $Gpf_i(s)$ stands for the vehicle position evolution in function of the reference acceleration. A lead-based controller is used to increase the response damping and ensure the required phase margin. To guarantee the same stability and response for any targeted time gap, a pole is added to the controller $C_i(s)$ at $\omega = -1/h rad/s$. In addition to this, robustness against the observed plant gain variations is considered as another control performance requirement.

System robustness is related to the ability to guarantee performance specifications with plant variations. These differences can be unexpected, like model uncertainties, or expected, like unmodeled dynamics. In any case, a robust controller must keep equivalent performance based on these specifications. Usual frequency domain constraints defining the system performance are shown in Eqs. (4) and (5), referring to gain crossover frequency ω_{cg} and phase margin ϕ_m specifications:

$$|C_i(j\omega_{cg})Gpf_i(j\omega_{cg})H_i(j\omega_{cg})|_{dB} = 0\,\text{dB}, \tag{4}$$

$$|\arg(C_i(j\omega_{cg})Gpf_i(j\omega_{cg})H_i(j\omega_{cg})) = -\pi + \phi_m, \tag{5}$$

Once ω_{cg} and ϕ_m are selected, these constraints are used for controller tuning, resulting in a controller that fits both equations. While ω_{cg} specifies desired responsiveness, ϕ_m is related to stability and overshoot. For our system, the following specifications granting a fast response with a low overshoot were chosen:

- $\omega_{cg} = 1\,\text{rad/s}$
- $\phi_m = 50\,\text{deg}$

Similar to works like [15,16,33,34], our robust control approach is to keep the stability specification described in Eq. (5) constant despite plant parameter variations. Flat phase slope, as defined in Eq. (6), is enough to fulfill this robustness constraint, yielding both a constant phase margin and a loop stability for different frequencies around the gain crossover frequency:

$$\left(\frac{d(\arg(C_i(j\omega)Gpf_i(j\omega)H_i(j\omega)))}{d\omega}\right)_{\omega=\omega_{cg}} = 0. \tag{6}$$

Fractional-order control fulfills this robustness constraint together with a phase margin specification. Therefore, a fractional-order controller is used in the control scheme of Fig. 2.

Our approach is based on the counter-slope method described in [29]. As a novelty in this work, an improvement of this methodology is proposed, allowing the user to choose a phase margin within the range of controller reachable margins by means of a graph, while the crossover frequency is directly computed, yielding an optimal solution by a simple tuning process and fulfilling all required control specifications.

Among the fractional-order controllers that can be tuned using this method are Fractional Proportional Derivative (*fPD*) and Fractional Proportional Integral (*fPI*). Due to the nature of our system and the required lead phase to stabilize car-following dynamics, the *fPD* formula shown in Eq. (7) will be used:

$$C_i(s) = k\frac{(1+\tau_a s^{\alpha})}{hs+1} = \frac{k_p + k_a s^{\alpha}}{hs+1}. \tag{7}$$

This controller includes the term $1/H_i(s)$ in order to cancel $H_i(s)$ dynamics, as discussed previously. Therefore, the resulting open loop transfer function is $L_i(s) = (k_p + k_a s^{\alpha})Gpf_i(s)$. Due to this cancellation, the term $H_i(s)$ will not be considered for the design of the controller, but added to the controller structure after the computation of its parameters k_p, k_a, and α.

Given the plant description and its frequency response, shown in Fig. 5, the slope of the phase at the gain crossover frequency is found to be $m_s = -33\,\text{deg}/\log(\omega)$, and the system phase $\phi_s = -195$ deg.

Therefore, according to the counter-slope method, the controller phase slope must be $m = 33\,\text{deg}/\log(\omega)$, and the phase addition needed to achieve the phase margin specified is $\phi_c = (-(-195) + 50 - 180)$ deg, $\phi_c = 65$ deg.

As discussed above, in this work we tackle the method's limitation by incorporating the phase margin specification into the design process, together with the crossover frequency and flat phase curve.

According to [29], the controller phase and phase slope can be defined through Eqs. (10) and (11) as follows:

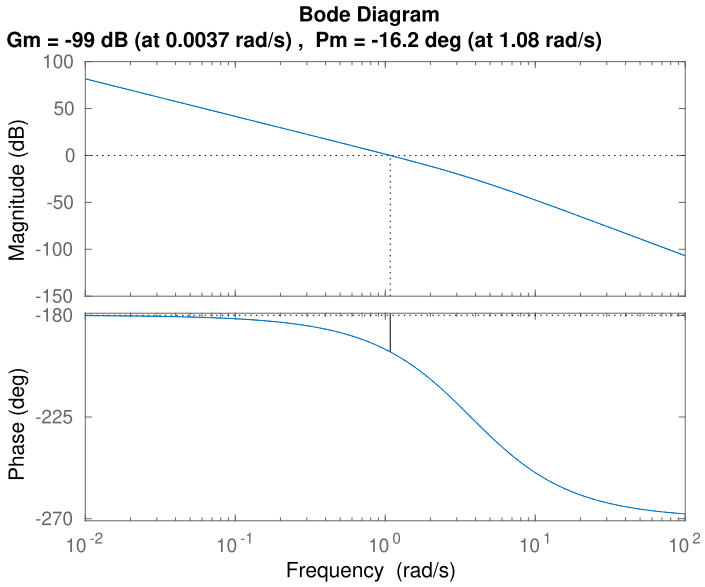

Fig. 5. Bode diagram of the open loop system $Gpf_i(s)$.

$$\phi_c(\omega) = \arctan\left(\frac{\sin(\alpha\pi/2)}{\frac{1}{\tau_a\omega^\alpha} + \cos(\alpha\pi/2)}\right), \tag{8}$$

$$m = \frac{d}{d\log_{10}(\omega)} \arctan\left(\frac{\sin(\alpha\pi/2)}{\frac{1}{\tau_a\omega^\alpha} + \cos(\alpha\pi/2)}\right). \tag{9}$$

Simplifying through a variable change of the form $\tau_x = 1/\tau_a\omega_{cg}^\alpha$ and solving the derivative results in:

$$\phi_c = \arctan\left(\frac{\sin(\alpha\pi/2)}{\tau_x + \cos(\alpha\pi/2)}\right), \tag{10}$$

$$m = \frac{\log(10)\cdot\alpha\cdot\sin(\alpha\pi/2)}{\tau_x + \frac{1}{\tau_x} + 2\cos(\alpha\pi/2)}. \tag{11}$$

In this work, a graphical method will be used to solve this nonlinear problem, as its nature permits straightforward controller retuning in case the control requirements or the plant dynamics are modified. This easy-to-tune graphic-based controller design method is a key contribution in this paper.

Fig. 6 offers a great insight into the controller parameters effects, giving clues on how to change them to enhance the response towards a particular direction. Solid lines show all τ_x values as a function of the exponent α according to Eq. (10) for different controller phases ϕ_c ranging from 0 deg ($\alpha = 0$) to 90 deg ($\alpha = 1$). Dashed lines in the same graph represent all valid solutions to Eq. (11) (τ_x cannot be a complex number) for the required slope, allowing to find the values of α and τ_x that fit both equations at once just by finding the intersection.

Using this method, given the required controller phase ($\phi_c = 65$ deg), the following values of $\alpha = 0.91$ and $\tau_x = 0.34$ are obtained from Fig. 6.

Once α and τ_x are known, τ_a is computed as:

$$\tau_a = \frac{1}{\tau_x\omega_{cg}^\alpha}, \tag{12}$$

resulting $\tau_a = 2.94$. Next, k is solved as a function of ω_{cg} through equation

$$k = \frac{1}{|1 + \tau_a j\omega_{cg}^\alpha||Gpf_i(j\omega_{cg})|}, \tag{13}$$

resulting a value $k = 0.2607$. Knowing all parameters the final controller is:

$$C_i(s) = 0.2607\frac{(1 + 2.94s^{0.91})}{hs + 1} = \frac{0.2607 + 0.7741s^{0.91}}{hs + 1}. \tag{14}$$

Fig. 7 shows the frequency response of the controlled system in open loop. One can observe how the Bode diagram shows fulfilled phase and frequency specifications while presenting a flat phase slope around the crossover frequency.

Simulation results

The time-domain controller performance was analyzed in simulation, including plant variations. Fig. 8 shows the step responses of the system for variations of the plant gain using the controller proposed. One can see how the performance is greatly improved, showing a constant overshoot, usually known as the iso-damping property.

Fig. 9 shows the developed controller tested in a simulation framework, where a 4-vehicle string is analyzed. First vehicle is set to track an acceleration profile, whereas followers are tracking the leader with the designed ACC controller at a time gap of $h = 1.5s$. Upper plot shows all vehicles' longitudinal speeds, middle plot depicts spacing error evolution and bottom figure presents the inter-vehicle distances. Vehicles in the string are set with different DC gain disturbances $\Delta \in [0.76, 1.3]$, where vehicles of index 1, 2, 3 and 4 are set with $\Delta = 1.0, 0.76, 1.1, 1.3$, respectively.

Changes of speed introduced by the leader are correctly tracked by the rest of the string, following the desired constant time gap policy. It is important to highlight that the achieved iso-damping property yields that all vehicles show the same stability and closed loop response overshoot, despite the different DC gains set for the vehicles. This guaranteed robustness is highly desirable for automated car-following systems, since a difference in road slope, vehicle mass or powertrain dynamics may produce these undesired disturbances.

For the sake of validation, the obtained string performance with the designed controller is compared to an integer-order PD controller (IOPD), which is designed to guarantee the same desired phase margin and crossover frequency. The obtained IOPD controller results of the form $C_i(s) = 0.373 + 0.7662s$. In Fig. 10, the frequency response of loop expression $Gp_{f,i}(s)C_i(s)H(s)$ is depicted for the integer-order PD controller (blue line) and the fractional-order controller (red line). Notice that although both fulfil the

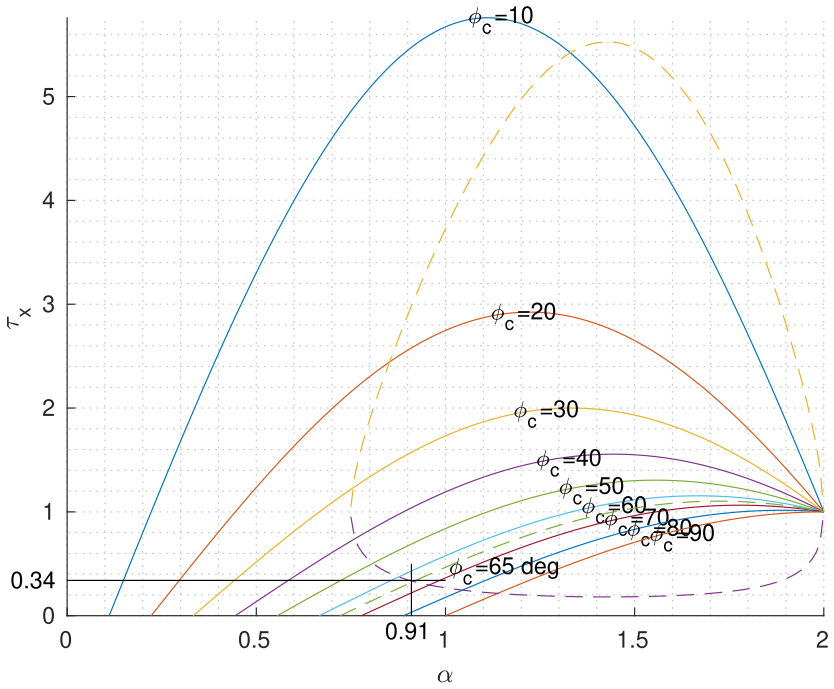

Fig. 6. Graph showing τ_x as a function of α according to Eq. (10) (solid lines) and Eq. (11) (dashed lines). Particular solution for $m = 33$ deg / log(ω) and $\phi_c = 65$ deg: the curves intersection shows values $\alpha = 0.91$ and $.\tau_x = 0.34$.

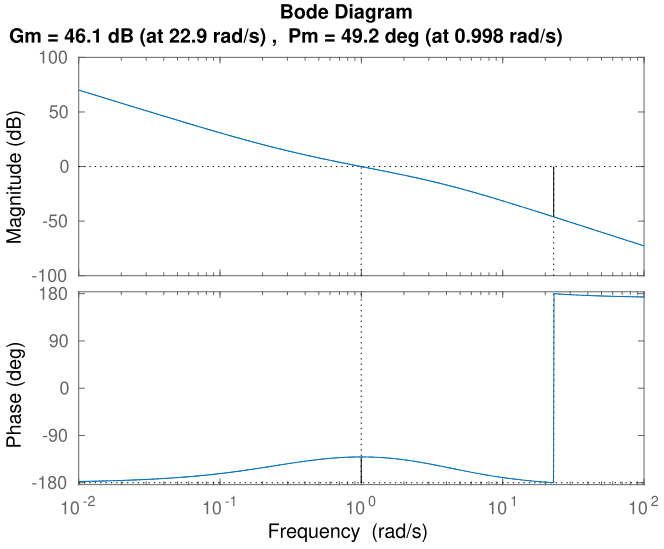

Fig. 7. Open loop Bode diagram of the controlled system designed using the improved counter-slope tuning method.

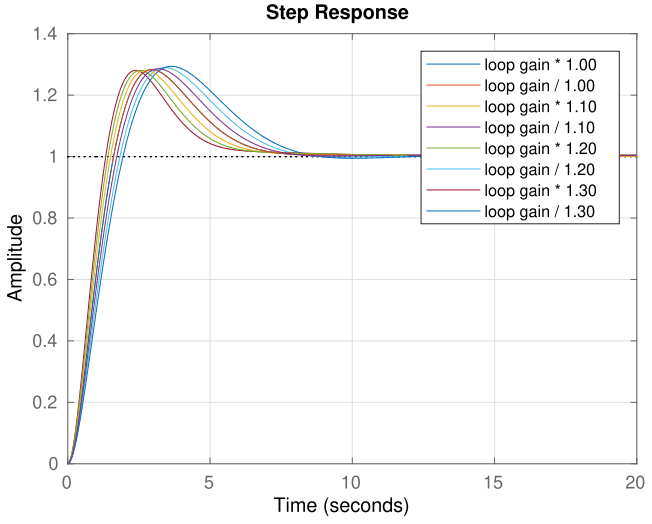

Fig. 8. Step response of the system with the fractional-order controller designed using the improved counter-slope tuning method. Gain range $(1.3G, \frac{1}{1.3}G)$, where G is the system default gain ($G = 1$).

phase margin and crossover frequency requirements, only the later yields a flat phase in the vicinity of the crossover frequency.

Fig. 11 shows the response of the fourth vehicle in the string when equipped with either the IOPD (blue line) or the FOPD (red line) controller. The top graph depicts vehicle's speed. The bottom plot shows the tracking error capabilities. The leader vehicle follows the same speed profile presented in Fig. 9. One can observe a slightly higher overshoot for the IOPD-vehicle, given that its gain has been altered by the disturbance Δ. Besides, not only the spacing error results more stable, but also the integrated absolute error is reduced by 17% when the fractional-order controller is used, instead of the IOPD. This capability is desirable, especially when dealing with string of heterogeneous dynamics. The iso-damping property would play a key role on guaranteeing a consistent car-following performance between vehicles.

Experimental results

The controller designed using the counter-slope method for the Honda Accord dynamics has been discretized and implemented on the vehicle real-time computer. Using the Tustin method to discretize at a sampling period of 0.05s, the high-level gap controller results:

$$C_i(z) = \frac{0.3621z^6 - 1.193z^5 + 1.087z^4 + 0.4256z^3 - 1.301z^2 + 0.7669z - 0.1482}{z^6 - 3.53z^5 + 3.937z^4 - 0.2446z^3 - 2.575z^2 + 1.788z - 0.3746} \quad (15)$$

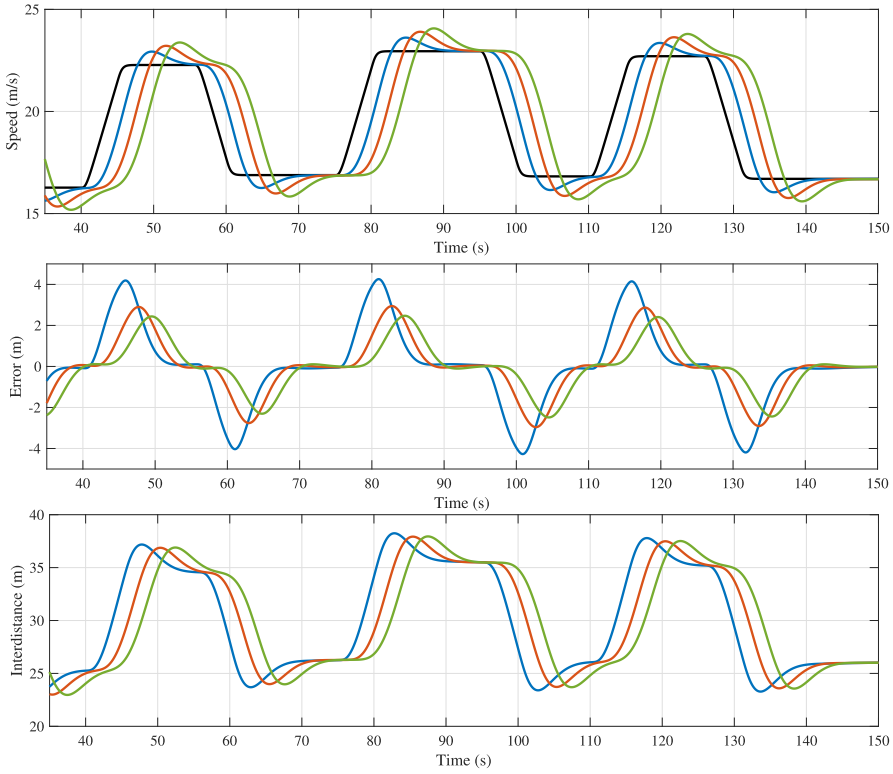

Fig. 9. Simulation results introducing plant DC gain disturbances on the run. Plotted variables belong to leader and controlled vehicles of index 2, 3 and 4 (black, blue, red and green lines, respectively).

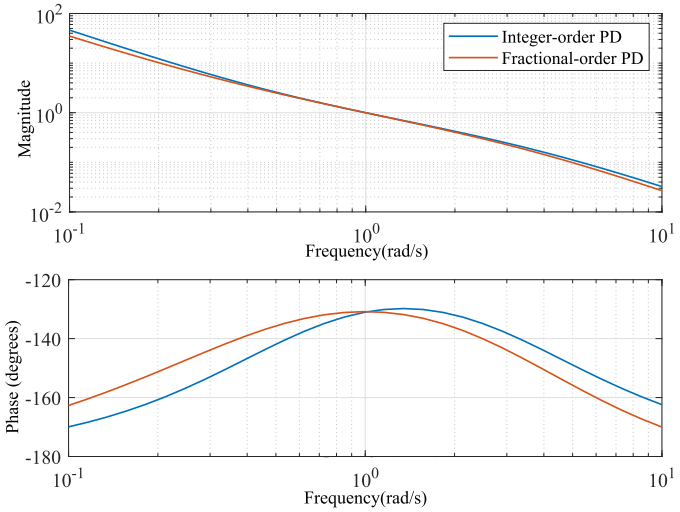

Fig. 10. Loop frequency responses when implementing the integer and fractional-order controllers.

The controller performance is implemented on the Hybrid Honda Accord 2014 platform in Fig. 4 and evaluated on a highway scenario. A target vehicle is tracked using front radar, aiming to keep a time gap of $h = 1.5s$. Fig. 12 shows preceding and subject vehicles' measured speeds. One can see that the controlled vehicle tracks accurately the speed oscillations coming from the preceding vehicle. Besides, not only incoming speed changes are tracked, but these are not being amplified, demonstrating the controller's capability to also ensure string stable car-following.

In Fig. 13, the measured spacing gap is plotted, which evolves proportionally to the subject vehicle's speed, following the adopted spacing policy with a time gap of 1.5s. The spacing error evolution is depicted in Fig. 14, showing an absolute value lower than 1.8 m. This demonstrates the algorithm potential to guarantee a safe and stable tracking, even at highway speeds and despite possible road slope changes that affect the low level system gain. It is important to highlight that the obtained experimental results are consistent with the simulated data presented previously, in terms of speed propagation and spacing error magnitudes. This confirms the approach feasibility and its benefits added to real world applications.

Conclusions and future works

This paper presents a novel graphical method that eases the control tuning process and demonstrates the potential of mixing fractional-order calculus with the loop iso-damping approach. This has been shown as a working solution to an important issue in the automated car-following field, which is rejecting possible disturbances on the low level response due to different dynamics, powetrains or road slope. A hierarchical ACC control structure has been utilized, where the fractional-order controller is in charge of regulating the distance gap through a reference acceleration tracked by a lower control layer. The proposed method allows not only to define intuitively the controller parameters that satisfy the design constraints, but also to observe at a glance how parameters modify the loop dynamics.

The algorithm has been applied considering vehicle and actuator dynamics of a Hybrid Honda Accord vehicle and its effectiveness has been demonstrated on both simulation environments and highway scenarios. The simulation results show that despite controlling a string vehicles with disturbed plant gains, the proposed controller performance is not only observed consistent, but also to outperform that one of an integer-order PD controller. The iso-damping potential to ensure robustness to gain changes

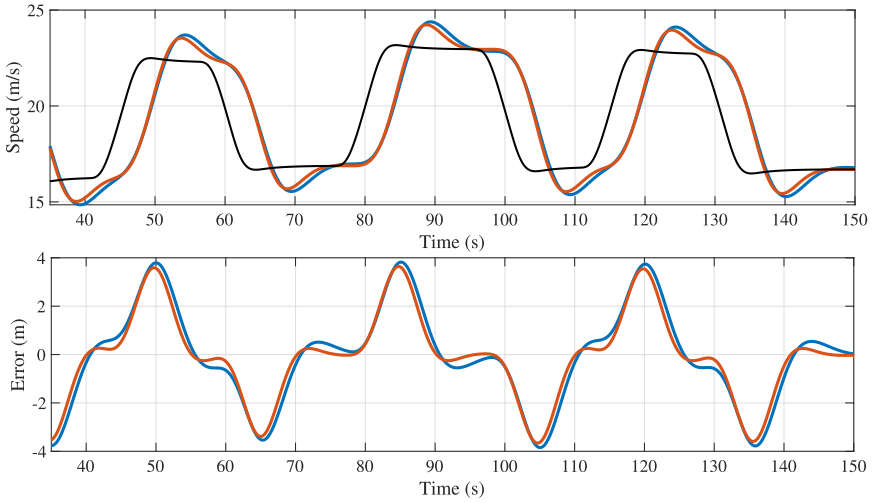

Fig. 11. Performance comparison showing last vehicle variables of ACC-controlled strings implementing IOPD (blue line) and fractional-order (red line) controllers.

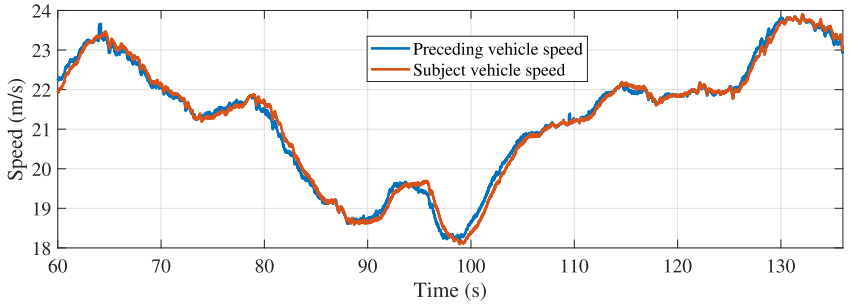

Fig. 12. Preceding and controlled vehicles' speeds.

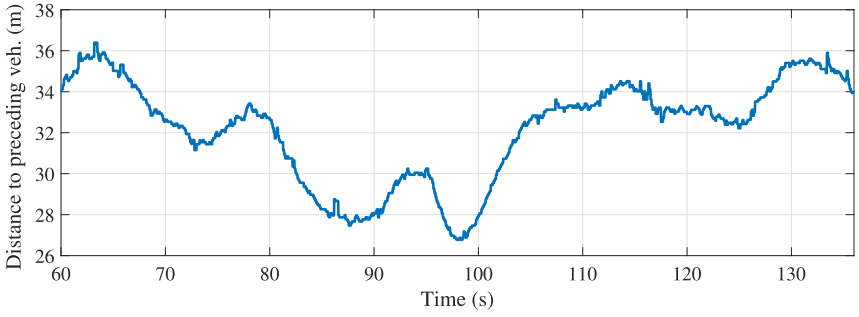

Fig. 13. Measured distance towards preceding vehicle.

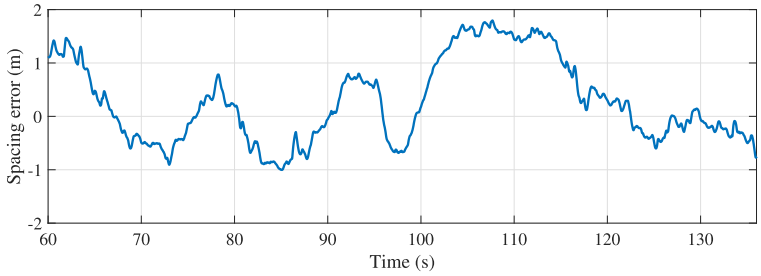

Fig. 14. Spacing gap error used for feedback control.

in the controlled plant has been therein confirmed, observing good performance and stability despite the actuator used to track the preceding vehicle's speed changes. The graphical nature of the proposed approach has showed how easily it could be applied to any type of vehicle dynamics, which is convenient to encourage vehicle automation adoption. Rejection of more complex disturbance structures, as well as car-following at shorter time gaps will be scoped in future works, by adding vehicle-to-vehicle communication links.

Compliance with Ethics Requirements

This article does not contain any studies with human or animal subjects.

Declaration of Competing Interest

The authors declare that they have no known competing financial interests or personal relationships that could have appeared to influence the work reported in this paper.

Acknowledgement

This research is supported by the Vehicle Technology Office (VTO), U.S. Department of Energy, under the Energy Efficient Mobility Systems (EEMS) initiative of the SMART Mobility Program, through the Lawrence Berkeley National Laboratory. The contents of this paper reflect the views of the authors, who are responsible for the facts and accuracy of the data presented herein.

References

[1] Schrank D, Eisele B, Lomax T. 2019 urban mobility scorecard, Tech. rep., Texas A&M Transportation Institute; 2019.
[2] Xiao L, Gao F. A comprehensive review of the development of adaptive cruise control systems. Vehicle Syst Dyn 2010;48(10):1167–92.
[3] Park S, Rakha H, Ahn K, Moran K. Fuel economy impacts of manual, conventional cruise control, and predictive eco-cruise control driving. Int J Transp Sci Technol 2013;2(3):227–42.
[4] Milanés V, Shladover SE. Modeling cooperative and autonomous adaptive cruise control dynamic responses using experimental data. Transp Res Part C: Emerg Technol 2014;48:285–300.
[5] Flores C, Milanés V. Fractional-order-based acc/cacc algorithm for improving string stability. Transp Res Part C: Emergi Technol 2018;95:381–93.
[6] Åström KJ, Hägglund T, Astrom KJ. Advanced PID control, vol. 461. ISA-The Instrumentation, Systems, and Automation Society Research Triangle; 2006.
[7] Sun Y, Wang X, Li L, Shi J, An Q. Modelling and control for economy-oriented car-following problem of hybrid electric vehicle. IET Intel Transp Syst 2019;13(5):825–33.
[8] Milanés V, Villagrá J, Pérez J, González C. Low-speed longitudinal controllers for mass-produced cars: A comparative study. IEEE Trans Industr Electron 2012;59(1):620–8.
[9] Gao F, Li SE, Zheng Y, Kum D. Robust control of heterogeneous vehicular platoon with uncertain dynamics and communication delay. IET Intel Transp Syst 2016;10(7):503–13.
[10] You H, Shen Y, Xing H, Yang S. Optimal control and parameters design for the fractional-order vehicle suspension system. J Low Freq Noise Vib Active Control 2018;37(3):456–67.
[11] Chen Q, Chen T, Yu H, Song J, Liu D. Lateral control for autonomous parking system with fractional order controller. JSW 2011;6(6):1075–81.
[12] Wang P, Wang Q, Wan M, Chen N. A fractional derivative-based lateral preview driver model for autonomous automobile path tracking. Math Probl Eng 2018.
[13] Tejado I, Milanés V, Villagrá J, Godoy J, HosseinNia H, Vinagre BM. Low speed control of an autonomous vehicle by using a fractional pi controller. IFAC Proc Vol 2011;44(1):15025–30.
[14] Hosseinnia SH, Tejado I, Milanés V, Villagrá J, Vinagre BM. Experimental application of hybrid fractional-order adaptive cruise control at low speed. IEEE Trans Control Syst Technol 2014;22(6):2329–36.
[15] Monje CA, Vinagre BM, Feliu V, Chen Y. Tuning and auto-tuning of fractional order controllers for industry applications. Control Eng Pract 2008;16(7):798–812.
[16] Petras I. Fractional order feedback control of a DC motor. J Electrical Eng 2009;60(3):117–28.
[17] Caponetto R, Dongola G. A numerical approach for computing stability region of fo-pid controller. J Franklin Inst 2013;350(4):871–89. doi: https://doi.org/10.1016/j.jfranklin.2013.01.017. http://www.sciencedirect.com/science/article/pii/S0016003213000343.
[18] Ranjbaran K, Tabatabaei M. Fractional order [pi], [pd] and [pi][pd] controller design using Bode's integrals. Int J Dyn Control 2018;6(1):200–12. doi: https://doi.org/10.1007/s40435-016-0301-7.
[19] Kennedy J, Eberhart R. Particle swarm optimization. In: Proceedings of IEEE international conference on neural networks, vol. 4; 1995. p. 1942–8. doi:10.1109/ICNN.1995.488968.
[20] Khandani K, Jalali AA. Robust fractional order control of a DC motor based on particle swarm optimization. In: MEMS, NANO and smart systems, Advanced Materials Research, vol. 403. Trans Tech Publications; 2012, p. 5030–7. doi:10.4028/www.scientific.net/AMR.403-408.5030.
[21] Rajasekhar A, Kunathi P, Abraham A, Pant M. Fractional order speed control of DC motor using Levy Mutated Artificial Bee Colony Algorithm. In: 2011 world congress on information and communication technologies. p. 7–13. doi: https://doi.org/10.1109/WICT.2011.6141192.
[22] Haji VH, Monje CA. Fractional order Fuzzy-PID control of a combined cycle power plant using Particle Swarm Optimization algorithm with an improved dynamic parameters selection. Appl Soft Comput 2017;58:256–64. doi: https://doi.org/10.1016/j.asoc.2017.04.033.
[23] Martín F, Monje CA, Moreno L, Balaguer C. DE-based tuning of PI^{λ} D^{μ} controllers. ISA Trans 2015;59:398–407. doi: https://doi.org/10.1016/j.isatra.2015.10.002.
[24] Monje CA, Vinagre BM, Feliu V, Chen Y. Tuning and auto-tuning of fractional order controllers for industry applications. Control Eng Pract 2008;16(7):798–812.
[25] Caponetto R, Dongola G, Pappalardo F, Tomasello V. Auto-tuning and fractional order controller implementation on hardware in the loop system. J Optim Theory Appl 2013;156(1):141–52.
[26] Luo Y, Chen Y. Fractional order PD controller tuning for position systems. John Wiley and Sons, Ltd; 2012, Ch. 6, p. 97–111. arXiv:https://onlinelibrary.wiley.com/doi/pdf/10.1002/9781118387726.ch6, doi:10.1002/9781118387726.ch6. https://onlinelibrary.wiley.com/doi/abs/10.1002/9781118387726.ch6.
[27] Muresan CI et al. Simplified optimization routine for tuning robust fractional order controllers. Am J Comput Math 2013;3(3):7–12. doi: https://doi.org/10.4236/ajcm.2013.33b002.
[28] Keyser RD, Muresan CI, Ionescu CM. A novel auto-tuning method for fractional order pi/pd controllers. ISA Trans 2016; 62: 268–275, sI: Control of Renewable Energy Systems. doi: 10.1016/j.isatra.2016.01.021. http://www.sciencedirect.com/science/article/pii/S0019057816000392.
[29] Muñoz J, Monje CA, Martínez de la Casa S, Balaguer C. Joint position control based on fractional-order PD and PI controllers for the arm of the humanoid robot teo, Int J Humanoid Robot 2019; 16 (06): 1950042. arXiv:https://doi.org/10.1142/S0219843619500427, doi:10.1142/S0219843619500427. doi: 10.1142/S0219843619500427.
[30] Flores C, Milanés V, Nashashibi F. A time gap-based spacing policy for full-range car-following. In: 2017 IEEE 20th International Conference on Intelligent Transportation Systems (ITSC). IEEE; 2017. p. 1–6.
[31] Rajamani R. Vehicle dynamics and control. Springer Science & Business Media; 2011.
[32] Sename O, Gaspar P, Bokor J. Robust control and linear parameter varying approaches: application to vehicle dynamics, Vol. 437. Springer; 2013.
[33] Qingshun T, Chunfu W, Yuanhui Y, Guodong L, Fengyu Z. Design and implementation of fractional order controller for service robots. Int J Control Automat 2015;8(5):209–20.
[34] Feliu V, Vinagre BM, Monje CA. Fractional-order control of a flexible manipulator. In: Sabatier J, Agrawal OP, Machado JAT, editors. Advances in fractional calculus: theoretical developments and applications in physics and engineering. Springer, vol. 1. Dordrecht: Netherlands; 2007. p. 449–62.